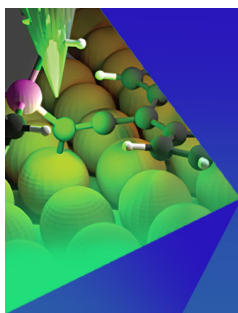# Structure and fragmentation of doubly ionized HNCS

Måns Wallner ; Emelie Olsson ; Veronica Ideböhn ; Marco Parriani ; Richard J. Squibb; Sven Lundberg ; Daniel Cole; Stefano Falcinelli ; Stefano Stranges ; Bruno Brunetti; John M. Dyke ; Gunnar Nyman ; John H. D. Eland; Majdi Hochlaf ; Raimund Feifel ✉

Check for updates

View Online

Export Citation

Structure and fragmentation of doubly ionized HNCS

Måns Wallner,[1] Emelie Olsson,[1] Veronica Ideböhn,[1] Marco Parriani,[1,2] Richard J. Squibb,[1]
Sven Lundberg,[1] Daniel Cole,[1] Stefano Falcinelli,[2] Stefano Stranges,[3,4] Bruno Brunetti,[4]
John M. Dyke,[5] Gunnar Nyman,[6] John H. D. Eland,[1,7] Majdi Hochlaf,[8,a] and Raimund Feifel[1,b]

AFFILIATIONS

[1] University of Gothenburg, Department of Physics, Origovägen 6B, 412 58 Gothenburg, Sweden

[2] University of Perugia, Department of Civil and Environmental Engineering, Via G. Duranti 93, 06125 Perugia, Italy

[3] CNR–Istituto Officina dei Materiali (IOM), Laboratorio TASC, 34149 Trieste, Italy

[4] Dipartimento di Chimica e Tecnologia dei Farmaci, Università Sapienza, Roma I-00185, Italy

[5] School of Chemistry, University of Southampton, Highfield, Southampton SO17 1BJ, United Kingdom

[6] University of Gothenburg, Department of Chemistry and Molecular Biology, Box 462, 405 30 Gothenburg, Sweden

[7] Oxford University, Department of Chemistry, Physical and Theoretical Chemistry Laboratory, South Parks Road, Oxford OX1 3QZ, United Kingdom

[8] Université Gustave Eiffel, COSYS/IMSE, 5 Bd Descartes, 77454 Champs sur Marne, France

[a] majdi.hochlaf@univ-eiffel.fr
[b] Author to whom correspondence should be addressed: raimund.feifel@physics.gu.se

ABSTRACT

Double ionization spectra of isothiocyanic acid (HNCS) have been measured using multi-electron and multi-ion coincidence techniques combined with high-level theoretical calculations. The adiabatic double ionization energy of HNCS is found at 27.1 ± 0.1 eV and is associated with the formation of the $X\,{}^3A''$ ground state of $HNCS^{2+}$. The characteristics of different dissociation channels are examined and compared to the results of electronic structure calculations obtained by systematically elongating the three bonds H–NCS, HN–CS, and HNC–S. For instance, the adiabatic double ionization energy of the NCS fragment is deduced to be 30.95 ± 0.5 eV. In addition, the C^+ and NS^+ dissociation channels are of particular interest, possibly indicating the involvement of a structural rearrangement process upon doubly ionizing HNCS.

INTRODUCTION

Isothiocyanic acid (HNCS) is the simplest isothiocyanate. Among the [H, N, C, S] isomeric family investigated numerically by several groups[1–3] in the past, HNCS is the most stable, closely followed by thiocyanic acid (HSCN), which is 0.26 eV higher in energy. Thiofulminic acid (HCNS) and isothiofulminic acid (HSNC) are 1.52 and 1.59 eV higher in energy than HNCS, respectively.

Beard and Dailey[4] were the first to determine the structure of neutral HNCS, using microwave spectroscopy to identify the sequence of atoms and initial bond lengths and angles. However, their results had significant errors, including overly long H–N bonds

and an inaccurately low H–N–C angle, due to the uncertainty in the value of the rotational constant A. Reid[5] later provided a more accurate value for A using infrared (IR) spectroscopy, which Beard and Dailey[6] incorporated together with the $(B + C)/2$ constant to refine their work. Dousmanis *et al.*[7] further improved the geometric structure by considering B–C values from microwave spectroscopy. In 1963, Kewley's microwave studies[8] successfully separated the B and C rotational constants, yielding even more refined structural parameters.

All early experimental studies assumed a strictly linear structure of the NCS chain; however, *ab initio* calculations[1] questioned this assumption, leading to a re-evaluation of the

structural parameters[9] in 1980. This study's modified substitution method revealed that the trans conformation is in actuality slightly bent, with bond lengths of r(H–N) = 0.993 Å, r(N–C) = 1.207 Å, r(C–S) = 1.5665 Å, and the angles ∠HNC = 131.7° and ∠NCS = 173.8°. The near-linear ∠NCS angle implies a quasi-linear character of HNCS, which complicated the determination of its equilibrium geometry for a long time.

HNCS was first detected in the interstellar medium[10] in the giant molecular cloud Sgr B2 in 1979, and subsequent studies have concretely established its presence in the interstellar medium.[11–14] Its significance in both interstellar and terrestrial environments has prompted numerous studies on neutral and singly charged HNCS. Photolysis of HNCS at low temperatures led to the first observations of its isomers, HSCN and HSNC.[15] Eland characterized the spectral bands of the single ionization photoelectron spectrum of HNCS in 1970.[16] Over twenty years later, Ruscic and Berkowitz[17] determined the appearance energy (AE) of singly charged fragments and the H–NCS bond energy. Gronowski's *ab initio* calculations confirmed the presence of neutral HNCS and its cation in the interstellar medium.[11]

The vibrational frequencies and structural parameters of HNCS have been calculated multiple times.[3,11,18,19] Electronic structure computations have explored the low-energy excited states of neutral HNCS, its singly charged cation,[20] and its neutral isomer HCNS,[19] along with studies on the entire HNCS isomeric family.[3] However, to our knowledge, the HNCS dication has not been previously studied.

This work presents the first experimental and theoretical investigation of the double ionization and subsequent fragmentation of HNCS upon single-photon absorption. Using a coincidence method, we detected mass-separated ionic fragments in correlation with all emitted electrons to gather kinetic energy information. The analysis of potential energy surfaces (PESs) in the electronic ground and excited states, both in the bound molecular region and near dissociation, provides a comprehensive understanding of the fragmentation processes of gas-phase $HNCS^{2+}$.

EXPERIMENTS

Multi-electron-multi-ion coincidence experiments were carried out at 40.81 eV photon energy provided by a pulsed He gas discharge lamp in Gothenburg and at 90 eV at the synchrotron radiation facility BESSY II in Berlin, well above the expected lowest double ionization energy of HNCS. The time-of-flight (TOF)-PEPEPIPICO apparatus used in the experiments has been described before.[21] In brief, it allows for the simultaneous detection of multiple electrons and multiple ions in coincidence. The time-of-flight (TOF) of all charged particles is recorded, and subsequently, the electron TOF is converted to kinetic energy while the ion TOF is converted to mass/charge. An effusive jet of the target gas is let into the chamber by a hollow needle of about 1.5 mm inner diameter to be intersected by wavelength selected light. The radiation source used in the Gothenburg laboratory is combined with a toroidal monochromator for selecting the 40.81 eV emission line, focusing the radiation on the light–matter interaction region with a spot size of about 1 mm in diameter. At BESSY-II, the VUV to soft x-ray beamline UE52-SGM was used, which provides a focus of about 0.5 mm in diameter. However, since at BESSY II, a mechanical chopper system was installed at the

radiation focus for adapting the light repetition rate to the requirements of our coincidence set-up while maintaining the photon flux, the spot size at the light–matter interaction region for these experiments was very similar to the spot size of the He lamp experiments in Gothenburg because of the divergence of the synchrotron radiation beam.

In the interaction region, upon ionization, the electrons are confined by a strong divergent magnetic field generated by a permanent magnet with a conically shaped pole piece before they enter a 2.2 m long drift tube surrounded by a solenoid, which provides a weak homogeneous magnetic field (about 1 mT) for guiding the electrons to a microchannel plate (MCP) detector. In experiments where only electrons are detected, a cylindrical permanent magnet provides a strong field (yielding 1.2 T at the conical tip and, depending on the actual tuning of the magnet position, between 0.7 and 1.0 T at the light–matter interaction region), resulting in a nominal resolving power of E/ΔE = 50. In the electron–ion coincidence configuration, a hollow cylindrical magnet is used instead; this results in a weaker field (about 0.1–0.2 T at the light–matter interaction point) and, thus, reduces the electron resolving power nominally to E/ΔE = 20. In this configuration, after about 150 ns, when all the relevant electrons have left the interaction zone, an electric field is applied across the region, extracting the ions in the opposite direction from the electrons. The ions are accelerated through the ring magnet into a 12 cm drift tube to travel to another MCP detector mounted in an in-line tandem configuration. The collection–detection efficiency for electrons is about 50%, and for ions, about 20%. To preserve proper coincidence conditions, the electron count rate is adjusted to about 2% of the light pulse rate. Operating, for instance, the pulsed He lamp at a 5 kHz repetition rate implies adjusting the gas pressure to 100 electron counts/second or lower, whereas the ion count rate is typically on the order of a few tens/second. Under such conditions, the typical data acquisition time is on the order of a few days.

The HNCS sample was prepared in the apparatus inlet system by heating a mixture of potassium thiocyanate and potassium bisulfate. The separate reagents were dried for several days over phosphorus pentoxide in a vacuum desiccator and then finely ground. The reagents were layered in a glass test tube with glass beads between layers and subsequently pumped using a rough vacuum for 24 h. The layers are kept in a vacuum and cooled in liquid nitrogen to be shaken vigorously until fully mixed. The purity of the different sample batches used was verified by on-line mass spectrometry, where the presence of carbonyl sulfide (OCS) and possibly some CO_2 were found to varying degrees, which was, in the worst case, up to 15% of the total data. This was taken into account in the data analysis, as explained further below.

THEORY

Ab initio electronic structure calculations were performed using the MOLPRO program suite.[22] In this work, we mapped the potential energy surfaces (PESs) of $HNCS^{2+}$ by elongating each bond separately and varying the angle ∠(HNC) (cf. supplementary material, Figs. S2–S13). While elongating the H–NCS and HN–CS bonds, we considered the eight lowest A′ and A″ states of singlet and triplet multiplicities, and for the HNC–S bond elongation, we treated the five lowest of these states of singlet and triplet

multiplicities. These computations were done in the C_s point group, where the A′ and A″ symmetries were treated equally. The PESs have been generated using the complete active space self-consistent field (CASSCF)[23,24] approach, followed by the explicitly correlated internally contracted multi-reference configuration interaction (MRCI-F12) method.[25] For this, we employed an active space of 7 orbitals within the valence shell. For the MRCI-F12 calculations, all configurations having a coefficient greater than 0.05 in the CI expansion of the CASSCF wave function were included in the reference, leading to more than 1.5×10^8 uncontracted configurations for the singlet electronic states and 3.5×10^8 uncontracted configurations for the triplet electronic states, per C_s symmetry. For these computations, the aug-cc-pVQZ basis set is used. Furthermore, to evaluate the adiabatic ionization energy and dissociation limits of $HNCS^{2+}$ forming $[H, N, C, S]^{2+}$, the partially spin restricted coupled cluster method, including perturbative triple excitations [RCCSD(T)],[26–28] is used. For the RCCSD(T) calculations, we used the aug-cc-pV(Q+d)Z and aug-cc-pV(5+d)Z basis sets of Dunning et al.[29–31] With two basis sets of the type aug-cc-pVXZ, where X = Q and 5, the complete basis set (CBS) is calculated using $E_X = E_{CBS} + A/X^3$, where A and E_{CBS} are the fitting parameters.[32,33] The PES cuts along the lowest energy angle ∠(HNC) are shown in Figs. 3–5, elongating the denoted bond length. For potential energy computations, all other bond lengths and angles are kept fixed at the values of the neutral HNCS geometry, with only the angle to the light-weight H being varied, which is faster moving and more sensitive. In addition to the PESs, the dissociation limits from the RCCSD(T) computations are shown. Finally, the cis–trans bending motions are calculated for fixed bond lengths and are shown in Fig. 6.

RESULTS AND DISCUSSION

A first step in the study of double ionization of HNCS is the coincidence detection of ion pairs formed upon fragmentation. An ion–ion coincidence map obtained at the photon energy of 40.81 eV in Gothenburg is presented in Fig. 1, where nine different dissociation channels are identified. Similar data were recorded at 90 eV photon energy in Berlin and are the basis for the breakdown data of $HNCS^{2+}$ summarized in Table I. The ion yields in this table
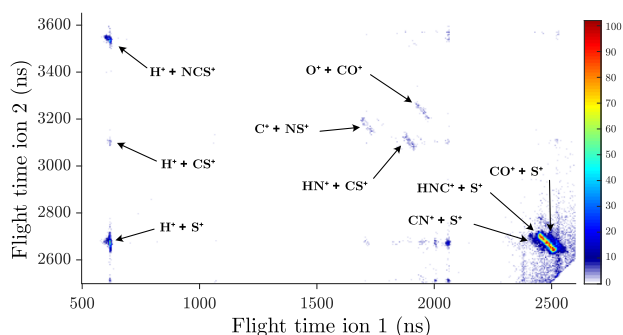
FIG. 1. Ion–ion coincidence map of HNCS taken at 40.81 eV photon energy. The spread in the time-of-flight of the coincidence islands contains information on the kinetic energy release involved in the dissociation processes.

TABLE I. Ion yields from ion–ion coincidence and doubly charged fragments from single events, normalized to $HNC^+ + S^+ = 100$. The doubly charged fragment yields are multiplied by 0.5 to account for the difference in collection efficiency in the normalization when only one fragment is detected.

Ion products	Ion yield at hν = 40.8 eV	Ion yield at hν = 90 eV
$HNC^+ + S^+$	100	100
$H^+ + NCS^+$	11.0	2.6
$HN^+ + CS^+$	6.9	6.9
$S^+ + CN^+$	16.2	39.2
$HS^+ + CN^+$	⋯	⋯
$H^+ + CS^+$	1.7	1.2
$H^+ + S^+$	15.7	12.3
$C^+ + NS^+$	3.7	4.7
$HNCS^{2+}$	123.0	173.0
NCS^{2+}	14.9	30.2
CS^{2+}	12.0	6.5

have been normalized to the yield of the strongest two-body breakdown channel, $HNC^+ + S^+$ (set to 100). In this table, the charge retaining decay channels with only one charged fragment are also included. These intensities have been factored by 0.5 to account for the difference in collection efficiency of the MCP as fewer fragments are detected for these channels. In addition, the putative decay channel $HS^+ + CN^+$ is artificially set to zero as it cannot unambiguously be selected in the ion–ion coincidence map. HS^+ with a mass of 33 and CN^+ with a mass of 26 are hidden by the much stronger $S^+ + HNC^+$ signals with the forward and backward spread in the time-of-flight of this channel due to the kinetic energy release (KER) involved.

To probe the electronic structure of doubly ionized HNCS, it is of great advantage to detect the two emitted electrons in coincidence. To select double ionization pathways for specific ions, it requires detection of the two electrons with at least one correlated ion in a three-fold coincidence. To unambiguously discuss cation pairs, four-fold coincidences are generally necessary, detecting both electrons and ions. This is especially true for larger molecules, where an undetected fragment may decay further into one charged and one neutral fragment.

Figure 2 shows the double ionization spectra of the decay channels with reasonable intensity in three- or four-fold coincidence together with the electron only data taken by a separate measurement. The CS^{2+} spectrum may have some interference from CO_2^{2+}, although it is believed to be rather small as the $CO^+ + O^+$ signal that would come from CO_2 is found to be weak. The CO^+ signal present is more strongly correlated with S^+, originating from OCS, which is estimated to account for 10%–15% of the total data. Apart from that, electron pairs extracted from three-fold coincidence events involving NS^+ (and C^+) are included instead of the much weaker electron pair data from four-fold events involving the $NS^+ + C^+$ pair.

For the assignment of the spectral features observed in Fig. 2, Table II also provides calculated vertical double ionization energies (DIEs) from the ground state of HNCS to populate the $HNCS^{2+}$ electronic states. Moreover, Table III presents the final states of the dicationic fragments calculated at the RCCSD(T)/CBS level
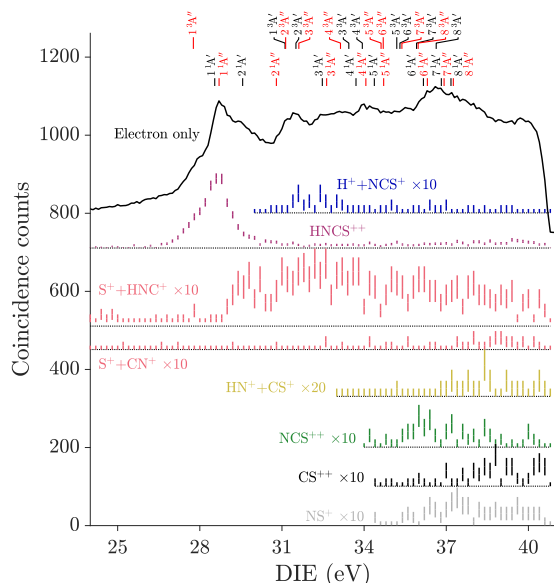
FIG. 2. Complete and ion channel specific double ionization electron pair spectra of HNCS using 40.81 eV photon energy. The electron only spectrum is represented by the solid black curve. The remaining spectra presented by using error bars are selected on either 1 or 2 ion(s), where the ions used for the selections are stated. The curves are scaled for visibility, and the statistics can be inferred from the range of the error bars (error = $\sqrt{N}$ and zero counts are given error = 1). The bar combs mark the vertical double ionization energies (DIEs) computed at the MRCI-F12/aug-cc-pVQZ level of theory at the neutral HNCS (X ^{1}A′) ground-state equilibrium geometry, as listed in Table II.

TABLE II. MRCI-F12/CASSCF/aug-cc-pVQZ vertical double ionization energies of HNCS to HNCS^{2+} quoted in C_s symmetry with respect to the energy at the equilibrium of HNCS (X ^{1}A′).

Electronic state	Energy (eV)
X ^{3}A″	27.77
1 ^{1}A′	28.57
1 ^{1}A″	28.70
2 ^{1}A′	29.57
2 ^{1}A″	30.80
1 ^{3}A′	31.11
2 ^{3}A″	31.13
2 ^{3}A′	31.51
3 ^{3}A″	31.62
3 ^{1}A′	32.47
3 ^{1}A″	32.63
4 ^{3}A″	33.14
3 ^{3}A′	33.44
4 ^{1}A′	33.70
4 ^{3}A′	33.94
4 ^{1}A″	34.06
5 ^{1}A′	34.37
5 ^{3}A″	34.62
6 ^{3}A″	34.70
5 ^{1}A″	34.71
5 ^{3}A′	35.19
6 ^{3}A′	35.31
7 ^{3}A″	35.38
7 ^{3}A′	35.92
8 ^{3}A″	35.97
6 ^{1}A′	36.17
6 ^{1}A″	36.31
8 ^{3}A′	36.63
7 ^{1}A′	36.82
7 ^{1}A″	36.92
8 ^{1}A′	37.17
8 ^{1}A″	37.26

relative to the initial neutral HNCS [including the zero-point vibrational energy (ZPE)], in comparison to the experimental values derived from Fig. 2. Where possible, the experimental fragmentation channels of sufficient statistics were extracted using four-fold coincidences, electron–electron–ion–ion (marked with a dagger in Table III). The remainders have too few counts, or, in the case of doubly charged fragments, only one detectable fragment. In addition, the KERs were calculated based on the field strength and time-of-flight width, utilizing the forward–backward separation of the peaks from two-fold ion–ion coincidences taken at 40.8 eV photon energy.

The first double ionization of HNCS has energy onsets experimentally observed at 27.1 ± 0.1 and 28.1 ± 0.3 eV, which agree reasonably well with the computed adiabatic values at 27.2 eV populating the X ^{3}A″ state and 28.5 eV populating the a ^{1}A″ state of HNCS^{2+}, listed in Table III. Following the work of Molloy et al.,[34] an empirical expression for the lowest double ionization energy of molecules is DIE = 2.2 × IE + $\frac{11.5}{r_{hh}}$, where r_{hh} denotes the distance between the two hole (h) vacancies. Hence, with a double ionization potential of 27.1 eV and a single ionization potential of 10.05 eV, known since the 1970s when it was experimentally determined by conventional valence photoelectron spectroscopy,[16] the distance between the valence holes in double ionization of HNCS can be estimated to be 2.3 Å (which is reasonable given the known equilibrium geometry of HNCS) and the optimized RCCSD(T)/aug-cc-pV(5+d)Z equilibrium geometry of HNCS^{2+} (X ^{3}A″) as depicted

in Fig. S1. We compute HN = 1.039 Å, NC = 1.149 Å, CS = 1.715 Å, HNC angle = 179.99°, NCS angle = 179.96°, and a torsion angle of 211.66°.

The decay channel HNC$^+$ + S$^+$ is the strongest two-body fragmentation channel and is found in Fig. 2 to have an experimental onset of about 29.1 ± 0.2 eV. To assist the interpretation, Fig. 3 shows potential energy surface (PES) cuts with elongation of the HNC–S bond in HNCS^{2+}. The lowest PES is that of the X ^{3}A″ state with a calculated appearance energy (AE) at the barrier of 29.26 eV, which is within the experimental error bars. The subsequent apparent peaks in the mass selected experimental data at 30.8, 31.5, and 33.0 eV are in good agreement with the subsequent PESs. The first and second excited states, 1 ^{1}A″ and 1 ^{1}A′, are very close together, and the lower ^{1}A″ has a curve crossing to the 1 ^{3}A′ and 2 ^{3}A″ states at 30.78 eV, or alternatively purely to the 1 ^{1}A″ state with its barrier at 30.86 eV. The third excited PES cut belongs to the 2 ^{1}A′ state

TABLE III. RCCSD(T)/CBS computations of the dissociation limits of HNCS fragmentation upon double ionization, with HNCS ground state as reference. These theoretical limits are compared to the thermodynamic thresholds primarily based on Lias *et al.*[36] and other sources cited. The theoretical appearance energy, the top of potential energy barriers, from Figs. 3–5, compared to the measured experimental onsets derived from the present double ionization electron spectra, where the dagger indicates values extracted from four-fold coincidences. The last column shows the experimental KERs estimated from ion–ion time-of-flight widths.

Final state	Diss. limit RCCSD(T)/CBS + ZPE (eV)	Heat of formation (eV)	Theory AE (eV)	Theory HNCS^{2+} X ^{3}A″ → KER (eV)	Expt. onset (eV)	Expt. KER (eV)
S$^+$ (^{2}D) + HNC$^+$ (X $^2\Sigma^+$)	27.9261	25.85[36–38]	29.26	→ ^{4}S + X $^2\Sigma^+$	29.1 ± 0.2[a]	3.2
S$^+$ (^{4}S) + HNC$^+$ (X $^2\Sigma^+$)	25.8545			3.41 eV		
S$^+$ (^{2}D) + HCN$^+$ (X $^2\Pi$)	28.8702					
S$^+$ (^{4}S) + HCN$^+$ (X $^2\Pi$)	26.7986	26.88[36]				
S$^+$ (^{2}D) + CN$^+$ ($^1\Sigma^+$) + H	34.5151				37.5 ± 1.0[a]	3.0
S$^+$ (^{4}S) + CN$^+$ ($^1\Sigma^+$) + H	32.4435	32.75[36]				
H$^+$ + NCS$^+$ (a $^1\Sigma^+$)	29.1490		30.90	→ X $^3\Pi$	31.2 ± 0.5[a]	<4.0
H$^+$ + NCS$^+$ (X $^3\Pi$)	28.1413	28.37[17,36]		2.8 eV		
HN$^+$ (X $^2\Sigma^+$) + CS$^+$ (X $^2\Sigma^+$)	30.0235	30.25[36]	33.50	→ X $^2\Sigma^+$ + X $^2\Sigma^+$	36.9 ± 1.0[a]	2.0
HN$^+$ (X $^2\Sigma^+$) + CS$^+$ (A $^2\Pi$)	33.5721			3.5 eV		
NCS^{2+} ($^2\Sigma^+$) + H	34.2965				35.0 ± 0.4	
NCS^{2+} ($^4\Pi$) + H	35.2456					
HNCS^{2+} (a ^{1}A″)	28.4932				28.1 ± 0.3	
HNCS^{2+} (X ^{3}A″)	27.2139				27.1 ± 0.1	
CH$^+$ (X $^1\Sigma^+$) + NS$^+$ (X $^1\Sigma^+$)	27.0843	27.09[36]				
CH$^+$ (a $^3\Pi$) + NS$^+$ (X $^1\Sigma^+$)	28.2863					
CH$^+$ (X $^1\Sigma^+$) + NS$^+$ (a $^3\Pi$)	31.5384					
CH$^+$ (a $^3\Pi$) + NS$^+$ (a $^3\Pi$)	32.7404					
C$^+$ (^{2}P) + NS$^+$ (X $^1\Sigma^+$) + H	31.1661	31.22[36]			36.2 ± 0.2[b]	2.9
C$^+$ (^{2}P) + NS$^+$ (a $^3\Pi$) + H	35.6203					
CS^{2+} (a $^1\Sigma$) + HN ($^3\Sigma^-$)	38.9031				38.0 ± 0.5	
CS^{2+} (X $^3\Pi$) + HN ($^3\Sigma^-$)	38.0446					
H$^+$ + S$^+$ (^{4}S) + CN (X $^2\Sigma^+$)	32.2428	32.25[36]			36.7 ± 0.4	

[a]The experimental onset was extracted in four-fold coincidences, implying less contamination but larger error bars.
[b]From the NS$^+$ fragment in three-fold coincidence.

and has a curve crossing to the 1 ^{3}A′ and 2 ^{3}A″ states at 31.5 eV. At higher energy, the density of states increases drastically, and no single curve can be selected.

The experimental KER increases with the double ionization energy, where the energy region of 29.0–30.4 eV corresponding to the first S$^+$ + HNC$^+$ peak in Fig. 2 has a KER = 2.5 eV, the second peak in the region of 30.8–34.4 eV has a KER = 2.8 eV, and the higher energy region of 34.8–39.4 eV has a KER = 3.8 eV. The computed KER from the maximum of the X ^{3}A″ PES to the limit S$^+$(^{4}S) + HNC$^+$(X $^2\Sigma^+$) is 3.4 eV, i.e., 1 eV higher than the first experimental onset KER. This may suggest that the HNC$^+$ fragment is given considerable rotational or vibrational energy, or it could imply the

isomerization of HNC$^+$ to HCN$^+$, which has its ground state about 1 eV higher in energy.

Figure 4 shows PES cuts with elongation of the H–NCS bond in HNCS^{2+}. The remaining bond lengths and angles are held at the geometry of neutral HNCS in its vibrational ground state, i.e., as they would be upon fast ionization. The lowest energy curve belongs to the X ^{3}A″ state, giving an AE of H$^+$ + NCS$^+$ at the maxima of the potential barrier at 30.93 eV, which, considering the comparatively large error bars, agrees reasonably with the experimental onset at 31.2 ± 0.5 eV. By referencing the dissociation limit at 28.15 eV, the theoretical KER is 2.78 eV. Going instead via the singlet states (1 ^{1}A′ or 1 ^{1}A″) with an AE of 31.8 eV yields a KER of 3.65 eV.
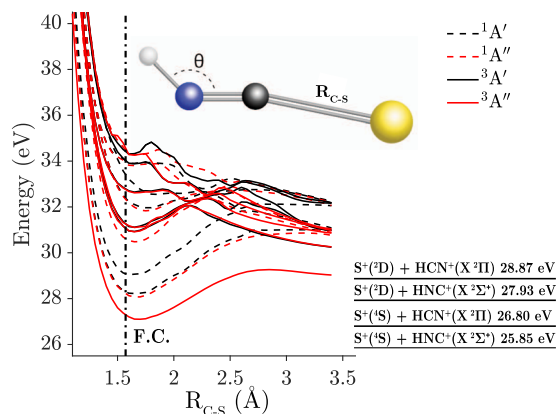
FIG. 3. The main part shows the potential energy curve extracted from the surface along the HNC–S bond distance in the HNCS dication, selecting the angle θ ($\angle$HNC) at each bond distance for the lowest energy. The curves are for in- and out-of-plane symmetry for the first five excited states of singlet and triplet spin multiplicity, calculated at the MRCI-F12/aug-cc-pVQZ level. The remaining bonds and angles are kept fixed at their values in the neutral ground state of HNCS (X ^{1}A′), HN = 1.0042 Å, NC = 1.2062 Å, and $\angle$NCS = 173.7°. The right part shows thermodynamic thresholds, using as a reference energy HNCS (X ^{1}A′) at equilibrium. F. C. corresponds to the middle of the Franck–Condon region (R_{C-S} = 1.57 Å) accessed from HNCS(X ^{1}A′).
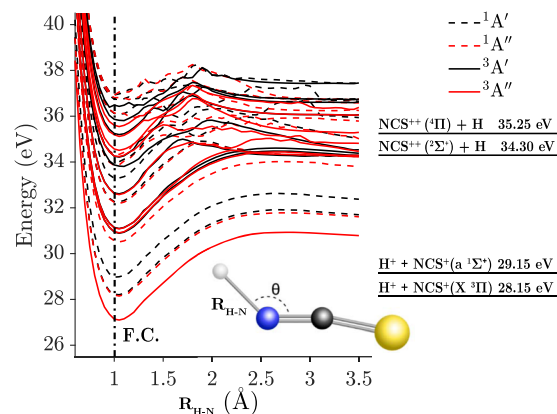
FIG. 4. The main part shows the potential energy curve extracted from the surface along the H–NCS bond distance in the HNCS dication, selecting the angle θ ($\angle$HNC) at each bond distance for the lowest energy. The curves are for in- and out-of-plane symmetry for the first eight excited states of singlet and triplet spin multiplicity, calculated at the MRCI-F12/aug-cc-pVQZ level. The remaining bonds and angles are kept fixed at their values in the neutral ground state of HNCS (X ^{1}A′), NC = 1.2062 Å, CS = 1.5718 Å, and $\angle$NCS = 173.7°. The right part shows thermodynamic thresholds, using as a reference energy HNCS (X ^{1}A′) at equilibrium. F. C. corresponds to the middle of the Franck–Condon region (R_{H-N} = 1.00 Å) accessed from HNCS(X ^{1}A′).

The latter is more plausible as the population of X ^{3}A″ is expected to go to the strongest dissociation channel. In both cases, the experimental KER is estimated to be less than 4 eV. However, two factors contribute to the uncertainty: the light H$^+$ species, given a few eV of kinetic energy, can move within 150 ns a few millimeters in the interaction zone before the ion extraction fields are applied, which may broaden the ion island, or the fast flying H$^+$ are easily lost in the apparatus and, thus, the peak shape is very diffuse. The slope of the coincidence island selected for H$^+$ + NCS$^+$ is −1, which is consistent with a two-body dissociation, implying that the correct part is chosen.

The NCS^{2+} channel is weak in the mass spectrum compared to the much stronger neighbors (m/z = 28 and 29.5), but with some careful selection, the experimental onset is determined to be 35.0 ± 0.4 eV. The RCCSD(T)/CBS computations suggest the lowest dissociation limit for H + NCS^{2+} at 34.3 eV for NCS^{2+} ($^2\Sigma^+$) and 35.25 eV for NCS^{2+} (a $^4\Pi$). In the mass spectrum, NCS^{2+} shows a narrower time-of-flight (TOF) width than its neighboring thermal parent ion, clearly implying a near zero KER, which is common for dissociation in the absence of Coulomb repulsion, as recently observed by us for the SO$_2$ → SO$_2^{2+}$ + O fragmentation channel.[35] This is also supported by the PESs clearly showing a high density of states at the energy of the asymptote. Unless, for some restricted reason , it is expected that the lowest limit will be reached. By using the known energy for bond cleavage of neutral H–NCS,[17] D_0 = 93.3 kcal/mol = 4.05 eV/particle, we can derive an estimate for the double ionization energy of NCS → NCS^{2+}, which here is computed using RCCSD(T)/CBS to 30.43 eV. Using E(HNCS) + AE(H + NCS^{2+}) = E(H) + E(NCS) + KER and E(HNCS) + D_0 = E(H) + E(NCS), the double ionization is estimated as DIE = E(NCS^{2+}) − E(NCS)

= AE(H + NCS^{2+}) − D_0 − KER. By using the experimental AE, the DIE of NCS^{2+} is found to be 30.95 ± 0.5 eV, fairly close to the 30.43 eV expected from theory. The experiment may somehow overestimate the double ionization energy of NCS by about the same amount as it does for the dissociation limit H + NCS^{2+}.

The experimental four-fold coincidence data of the HN$^+$ + CS$^+$ channel shown in Fig. 2 have somewhat limited statistics (thus leading to comparatively large error bars) but suggest the signal to rise around DIE = 36.9 ± 1 eV, with a stronger increase at 38 eV. Figure 5 shows PES cuts with elongation of the HN-CS bond in HNCS^{2+}. The first potential energy barrier has a maximum of 33.47 eV, providing the theoretical AE for HN$^+$ + CS$^+$, much lower than the experimental finding. From the X ^{3}A″ state barrier to the dissociation limit, there is about 3.5 eV left over for KER. The experimental KER extracted from the HN$^+$ + CS$^+$ ion–ion coincidence island (cf. Fig. 1) is about 2 eV, well below the theoretical value, possibly suggesting some internal energy for the final fragments. A possible explanation is that the fragmentation primarily leads to the final product at 33.57 eV via one of the many pathways in the energy region of 35–36.8 eV. Such a pathway is in better agreement with the low kinetic energy release and may be plausible; however, competitive curve crossings in the cis and trans bent structures, cf. Fig. 6, may prohibit this.

Apart from that, according to Fig. 2, the formation of CS^{2+} has its first significant increase in intensity around 38 eV. This does agree well with the dissociation limit from the computations (cf. Fig. 5), although the CS^{2+} is not reachable within the energy range where the PESs are calculated. The high density of states up to 37.9 eV leads one to believe that this trend may continue such that the dissociation
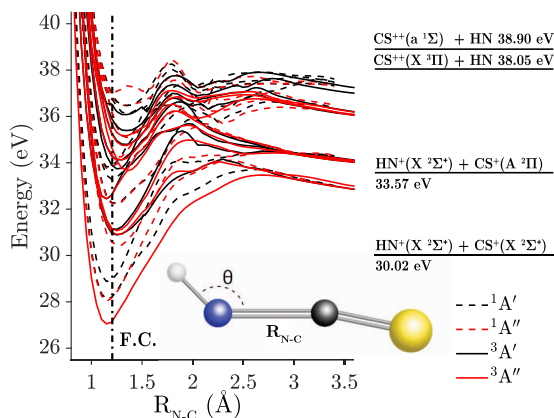
FIG. 5. The main part shows the potential energy curve extracted from the surface along the HN-CS bond distance in the HNCS dication, selecting the angle θ ($\angle$HNC) at each bond distance for the lowest energy. The curves are for in- and out-of-plane symmetry for the first eight excited states of singlet and triplet spin multiplicity, calculated at the MRCI-F12/aug-cc-pVQZ level. The remaining bonds and angles are kept fixed at their values in the neutral ground state of HNCS (X ^{1}A'), HN = 1.0042 Å, CS = 1.5718 Å, and $\angle$NCS = 173.7°. The right part shows thermodynamic thresholds, using as a reference energy HNCS (X ^{1}A') at equilibrium. F. C. corresponds to the middle of the Franck–Condon region (R_{N-C} = 1.21 Å) accessed from HNCS(X ^{1}A').
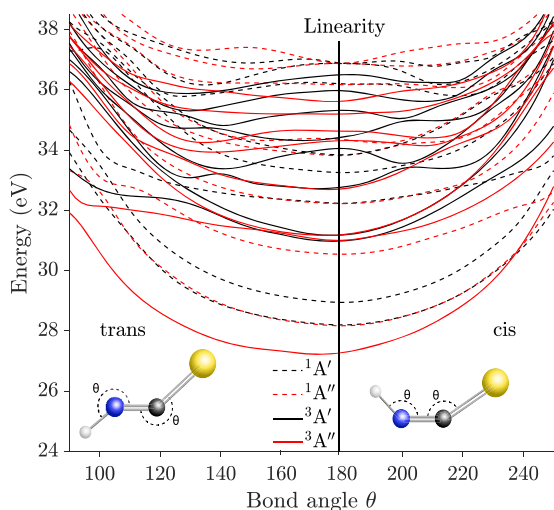
FIG. 6. MRCI-F12/CASSCF/aug-cc-pVQZ potential energy curves of the singlet and triplet electronic states of HNCS^{2+} by bending symmetrically at both in-plane angles θ for trans (left side) and cis (right side). The bond lengths are kept fixed at the geometry of the neutral HNCS (X ^{1}A') in its vibrational ground state.

limits are reached with a low KER, which is typical when only one of the fragments carries on the two charges.[35]

Figure 2 also provides details on the formation of the somewhat exotic NS$^+$ fragment, which must involve some bond rearrangement, either during photoionization or prior to the neutral molecule.

The stable neutral isomers with NS adjacent are the linear form HCNS or the bent HSNC at 1.52 and 1.58 eV, respectively, above the ground state HNCS.[3] Figure 2 and Table III suggest the three-fold coincidence onset of the NS$^+$ fragment, correlating with C$^+$, to be at 36.2 ± 0.2 eV. There is also a second discernible peak arising at 37.0 eV, but it would be very unusual to find distinct thresholds with the high density of molecular states present. There is some signal at 35.0 eV not correlating with C$^+$ in three-fold or four-fold coincidences, which is likely due to overlap in the ion spectrum with neighboring masses of considerable spread due to kinetic energy release. Another possibility is the production of NS$^+$ + H$^+$ + C with a 2.3 eV higher dissociation limit due to the difference in ionization potentials between C and H. The onsets at 36.2 and 37.0 eV are in agreement with the formation of the neutral carbon fragment and in poorer agreement with the formation of the extremely weak fourfold coincidence channel C$^+$ + NS$^+$. This channel is very clear in the ion–ion coincidence map, where the experimental KER can be estimated to be 2.9 eV. This puts the experimentally estimated dissociation limits at 33.3 and 34.1 eV, higher than the lowest dissociation limit at 31.16 eV. It is not likely for the carbon fragment to end up in an excited state, as the C$^+$ ^{4}P state is 5.3 eV above the ^{2}P state listed. It is possible that some of the extra 2–3 eV end up as kinetic energy for the neutral H fragment or as vibrational energy for the NS$^+$ fragment. Alternatively, photoionization directly from the isomer forms HCNS or HSNC would yield a lower dissociation limit and, hence, would make the discrepancy even larger.

Figure 6 shows cuts of singlet and triplet states along the bending coordinates. These cuts are obtained at the MRCI-F12/CASSCF/aug-cc-pVQZ level of theory by bending symmetrically both in-plane angles for trans and cis configurations. This shows that most of these states below 35 eV display monotonic behavior in the region where the molecular structure gets linear and where most states are minimized close to this configuration. This means that no bond rearrangements are expected until 35 eV, which is supported by the weaker dissociation channel producing C$^+$ and NS$^+$, which appears above 36 eV ionization energy (cf. NS$^+$ in Fig. 2). The C$^+$ + NS$^+$ is very weak in the four-fold coincidences but is seen clearly in the ion–ion coincidence map (cf. Fig. 1) at a KER of 2.9 eV. Moreover, this figure shows that all the doubly degenerate electronic states at linearity split into two components for bent structures. These components are thus coupled by Renner–Teller effects, and for the triplet, by spin–orbit in addition to the Renner–Teller effect. These effects couple these electronic states and favor the mixing of their wavefunctions. For bent structures, additional vibronic and spin–orbit coupling may play a role. Accordingly, the dynamics of fragmentation of HNCS^{2+} are viewed as very complex, and this may explain the internal (electronic, vibrational, or rotational) energy carried away by some fragments, as outlined above.

CONCLUSIONS

The formation and unimolecular decay of HNCS^{2+} have been investigated by three- and four-fold electron–ion coincidence spectroscopy and using advanced *ab initio* methods for data interpretation. We have found the doubly charged parent ion HNCS^{2+} to be stable and produced in high yield in the 27–30 eV region. The most

29 August 2024 10:56:18

favored dissociation channel is breaking the HNC–S bond starting from 29.1 eV all the way up to the photon energy, with increasing kinetic energy release. Several weaker dissociation channels were found, in particular the somewhat surprising NS^+ fragment, which may indicate the involvement of a structural rearrangement following the removal of two electrons. No final explanation can yet be given for the appearance of this fragment.

SUPPLEMENTARY MATERIAL

The complete results of the numerical calculations of the potential energy surfaces of $HNCS^{2+}$ by elongating each bond separately and varying the angle $\angle(HNC)$ are provided in the form of a separate supplementary material document.

ACKNOWLEDGMENTS

AUTHOR DECLARATIONS

Conflict of Interest

The authors have no conflicts to disclose.

Author Contributions

R.F. and J.H.D.E. devised the research project. S.S., B.B., and J.M.D. worked on the initial sample synthesis, which was subsequently refined by J.H.D.E., M.P., and R.J.S. M.W., E.O., V.I., M.P., S.S., R.J.S., S.L., D.C., and R.F. conducted the experimental research. M.W., S.L., D.C., and J.H.D.E. performed the data analysis. M.H. and M.W. carried out the theoretical calculations with the involvement of G.N. All authors discussed the results and contributed to writing the manuscript at several instances.

Måns Wallner: Conceptualization (lead); Data curation (equal); Formal analysis (lead); Funding acquisition (lead); Investigation (lead); Project administration (lead); Resources (lead); Supervision (lead); Writing – original draft (lead); Writing – review & editing (equal). **Emelie Olsson**: Data curation (equal); Formal analysis (lead); Investigation (supporting); Writing – original draft (lead); Writing – review & editing (equal). **Veronica Ideböhn**: Data curation (equal); Investigation (supporting); Writing – review & editing (equal). **Marco Parriani**: Data curation (equal); Investigation (supporting); Writing – review & editing (equal). **Richard J. Squibb**: Data curation (equal); Investigation (supporting); Supervision (supporting); Writing – review & editing (equal). **Sven Lundberg**: Data curation (equal); Investigation (supporting); Supervision (supporting); Writing – review & editing (equal). **Daniel Cole**: Data curation (equal); Investigation (supporting); Writing – review & editing (equal). **Stefano Falcinelli**: Data curation (equal); Investigation (supporting); Supervision (equal); Writing – review & editing (equal). **Stefano Stranges**: Data curation (equal); Investigation (equal); Supervision (supporting); Writing – review & editing (equal). **Bruno Brunetti**: Data curation (equal); Investigation (supporting); Supervision (supporting); Writing – review & editing (equal). **John M. Dyke**: Conceptualization (supporting); Investigation (supporting); Writing – review & editing (equal). **Gunnar Nyman**: Data curation (supporting); Investigation (supporting); Writing – review & editing (equal). **John H. D. Eland**: Conceptualization (equal); Data curation (supporting); Formal analysis (equal); Investigation (supporting); Supervision (supporting); Writing – original draft (equal); Writing – review & editing (equal). **Majdi Hochlaf**: Conceptualization (equal); Data curation (equal); Formal analysis (equal); Investigation (equal); Supervision (equal); Writing – original draft (equal); Writing – review & editing (equal). **Raimund Feifel**: Conceptualization (lead); Data curation (equal); Formal analysis (equal); Funding acquisition (lead); Project administration (lead); Resources (lead); Supervision (lead); Writing – original draft (equal); Writing – review & editing (equal).

DATA AVAILABILITY

The data that support the findings of this study are available from the corresponding author upon reasonable request.

REFERENCES

[1] B. Bak, J. J. Christiansen, O. J. Nielsen, and H. Svanholt, "Comparable ab initio calculated energies of HCNS, CNSH, NCSH and HNCS. Optimized geometries and dipole moments," Acta Chem. Scand. **31a**, 666–668 (1977).

[2] M. Wierzejewska and J. Moc, "Isomerization and dissociation of CHNS: Quantum mechanical study," J. Phys. Chem. A **107**, 11209–11216 (2003).

[3] B. A. McGuire *et al.*, "Molecular polymorphism: Microwave spectra, equilibrium structures, and an astronomical investigation of the HNCS isomeric family," Phys. Chem. Chem. Phys. **18**, 22693–22705 (2016).

[4] C. I. Beard and B. P. Dailey, "Microwave spectrum and structure of isothiocyanic acid," J. Chem. Phys. **15**, 762 (1947).

[5] C. Reid, "The infra-red absorption spectrum of isothiocyanic acid (HNCS)," J. Chem. Phys. **18**, 1512 (1950).

[6] C. I. Beard and B. P. Dailey, "The structure and dipole moment of isothiocyanic acid," J. Chem. Phys. **18**, 1437–1441 (1950).

[7] G. C. Dousmanis, T. M. Sanders, C. H. Townes, and H. J. Zeiger, "Structure of HNCS from microwave spectra," J. Chem. Phys. **21**, 1416 (1953).

[8] R. Kewley, K. V. L. N. Sastry, and M. Winnewisser, "The millimeter wave spectra of isocyanic and isothiocyanic acids," J. Mol. Spectrosc. **10**, 418–441 (1963).

[9] K. Yamada, M. Winnewisser, G. Winnewisser, L. Szalanski, and M. Gerry, "Ground state spectroscopic constants of $H^{15}NCS$, $HN^{13}CS$, and $HNC^{34}S$, and the molecular structure of isothiocyanic acid," J. Mol. Spectrosc. **79**, 295–313 (1980).

[10] M. A. Frerking, R. A. Linke, and P. Thaddeus, "Interstellar isothiocyanic acid," Astrophys. J. **234**, L143–L145 (1979).

[11] M. Gronowski and R. Kolos, "A theoretical study on the interstellar synthesis of H_2NCS^+ and $HNCSH^+$ cations," Astrophys. J. **792**, 89 (2014).

[12] W. M. Irvine, "The composition of interstellar molecular clouds," Space Sci. Rev. **90**, 203–218 (1999).

[13] D. T. Halfen *et al.*, "Detection of a new interstellar molecule: Thiocyanic acid HSCN," Astrophys. J. **702**, L124 (2009).

[14] G. R. Adande, D. T. Halfen, L. M. Ziurys, D. Quan, and E. Herbst, "Observations of the [HNCS]/[HSCN] ratio in Sgr B2 and TMC-1: Evidence for low-temperature gas-phase chemistry," Astrophys. J. **725**, 561 (2010).

[15] M. Wierzejewska and Z. Mielke, "Photolysis of isothiocyanic acid HNCS in low-temperature matrices. Infrared detection of HSCN and HSNC isomers," Chem. Phys. Lett. **349**, 227–234 (2001).

[16] J. H. D. Eland, "The photoelectron spectra of isocyanic acid and related compounds," Philos. Trans. R. Soc. London, Ser. A **268**, 87–96 (1970).

[17] B. Ruscic and J. Berkowitz, "The H–NCS bond energy, ΔH°_f (HNCS), ΔH°_f (NCS), and IP(NCS) from photoionization mass spectrometric studies of HNCS, NCS, and (NCS)$_2$," J. Chem. Phys. **101**, 7975–7989 (1994).

[18] J. R. Durig, C. Zheng, and H. Deeb, "On the structural parameters and vibrational spectra of some XNCS and XSCN (X = H, F, Cl, Br) molecules," J. Mol. Struct. **784**, 78–92 (2006).

[19] C. P. Kong, Z. X. Zhao, and H. X. Zhang, "Theoretical computation of low-lying electronic states of HCNS: A CASPT2 study," Int. J. Quantum Chem. **113**, 1416–1421 (2013).

[20] T. Liu, Z. X. Zhao, M. X. Song, H. X. Zhang, and C. C. Sun, "Low-lying electronic states of HNCS and its ions: A CASSCF/CASPT2 study," Theor. Chem. Acc. **128**, 215–222 (2011).

[21] J. H. D. Eland and R. Feifel, "Double ionisation of ICN and BrCN studied by a new photoelectron–photoion coincidence technique," Chem. Phys. **327**, 85–90 (2006).

[22] H.-J. Werner et al., MOLPRO, version 2019.2, a package of ab initio programs, 2019.

[23] P. J. Knowles and H.-J. Werner, "An efficient second-order MC SCF method for long configuration expansions," Chem. Phys. Lett. **115**, 259–267 (1985).

[24] H. Werner and P. J. Knowles, "A second order multiconfiguration SCF procedure with optimum convergence," J. Chem. Phys. **82**, 5053–5063 (1985).

[25] T. Shiozaki, G. Knizia, and H.-J. Werner, "Explicitly correlated multireference configuration interaction: MRCI-F12," J. Chem. Phys. **134**, 034113 (2011).

[26] C. Hampel, K. A. Peterson, and H. Werner, "A comparison of the efficiency and accuracy of the quadratic configuration interaction (QCISD), coupled cluster (CCSD), and Brueckner coupled cluster (BCCD) methods," Chem. Phys. Lett. **190**, 1–12 (1992).

[27] M. J. O. Deegan and P. J. Knowles, "Perturbative corrections to account for triple excitations in closed and open shell coupled cluster theories," Chem. Phys. Lett. **227**, 321–326 (1994).

[28] P. J. Knowles, C. Hampel, and H.-J. Werner, "Erratum: 'Coupled cluster theory for high spin, open shell reference wave functions' [J. Chem. Phys. 99, 5219 (1993)]," J. Chem. Phys. **112**, 3106–3107 (2000).

[29] R. A. Kendall, T. H. Dunning, and R. J. Harrison, "Electron affinities of the first-row atoms revisited. Systematic basis sets and wave functions," J. Chem. Phys. **96**, 6796–6806 (1992).

[30] D. E. Woon and T. H. Dunning, "Gaussian basis sets for use in correlated molecular calculations. III. The atoms aluminum through argon," J. Chem. Phys. **98**, 1358–1371 (1993).

[31] T. H. Dunning, K. A. Peterson, and A. K. Wilson, "Gaussian basis sets for use in correlated molecular calculations. X. The atoms aluminum through argon revisited," J. Chem. Phys. **114**, 9244–9253 (2001).

[32] T. Helgaker, W. Klopper, H. Koch, and J. Noga, "Basis-set convergence of correlated calculations on water," J. Chem. Phys. **106**, 9639–9646 (1997).

[33] C. Puzzarini, "Extrapolation to the complete basis set limit of structural parameters: Comparison of different approaches," J. Phys. Chem. A **113**, 14530–14535 (2009).

[34] R. D. Molloy, A. Danielsson, L. Karlsson, and J. H. D. Eland, "Double photoionisation spectra of small molecules and a new empirical rule for double ionisation energies," Chem. Phys. **335**, 49–54 (2007).

[35] M. Jarraya et al., "State selective fragmentation of doubly ionized sulphur dioxide," Sci. Rep. **11**, 17137 (2021).

[36] S. Lias et al., Gas-Phase Ion and Neutral Thermochemistry, Journal of Physical and Chemical Reference Vol. 17 (American Chemical Society and American Institute of Physics, 1988).

[37] A. Hansel, C. Scheiring, M. Glantschnig, W. Lindinger, and E. E. Ferguson, "Thermochemistry of HNC, HNC$^+$, and CF$_3^+$," J. Chem. Phys. **109**, 1748–1750 (1998).

[38] B. Gans et al., "Origin band of the first photoionizing transition of hydrogen isocyanide," Phys. Chem. Chem. Phys. **21**, 2337–2344 (2019).